ResearchGate

See discussions, stats, and author profiles for this publication at: https://www.researchgate.net/publication/230721551

Role of Propionates in Substrate Binding to Heme Oxygenase from Neisseria meningitidis: A Nuclear Magnetic Resonance Study

ARTICLE *in* BIOCHEMISTRY · AUGUST 2012

Impact Factor: 3.02 · DOI: 10.1021/bi3007803 · Source: PubMed

CITATIONS
2

READS
17

6 AUTHORS, INCLUDING:

Dungeng Peng
Vanderbilt University
21 PUBLICATIONS **177** CITATIONS
SEE PROFILE

Li-Hua Ma
23 PUBLICATIONS **234** CITATIONS
SEE PROFILE

Available from: Dungeng Peng
Retrieved on: 24 January 2016

NIH Public Access
Author Manuscript
Biochemistry. Author manuscript; available in PMC 2012 December 05.

Published in final edited form as:
Biochemistry. 2012 September 11; 51(36): 7054–7063. doi:10.1021/bi3007803.

The role of propionates in substrate binding to heme oxygenase from *Neisseria meningitidis*; A NMR study[†]

Dungeng Peng[#], **Li-Hua Ma**[#], **Kevin M. Smith**[#], **Xuhong Zhang**[‡], **Michihiko Sato**[‡ ‡], and **Gerd N. La Mar**[#,*]
Department of Chemistry, University of California, Davis, CA 95616; Department of Biochemistry and Molecular Biology, Yamagata University Graduate School of Medical Science, Yamagata 990-9585, Japan and Central Laboratory for Research and Education, Yamagata University Faculty of Medicine,Yamagata 990-9585, Japan

[#]Department of Chemistry, University of California, Davis

[‡]Department of Biochemistry and Molecular Biology, Yamagata University Graduate School of Medical Science, Yamagata 990-9585, Japan

[‡ ‡]Central Laboratory for Research and Education, Yamagata University Faculty of Medicine,Yamagata 990-9585, Japan

Abstract

Heme oxygenase, HO, cleaves hemin into biliverdin, iron and CO. For mammalian HOs, both native hemin propionates are required for substrate binding and activity. The HO from the pathogenic bacterium *Neisseria meningitidis*, *Nm*HO, possesses a crystallographically undetected C-terminal fragment that by solution ^{1}H NMR is found to fold and interact with the active site. One of the substrate propionates has been proposed to form a salt bridge to the C-terminus rather than to the conventional buried cationic side chain in other HOs. Moreover, the C-terminal dipeptide Arg208His209 cleaves spontaneously over ~24 hours at a rate dependent on substituent size. 2D ^{1}H NMR of *Nm*HO azide complexes with hemins with selectively deleted or rearranged propionates all bind to *Nm*HO with a structurally conserved active site as reflected in optical spectra and NMR NOESY cross peak and hyperfine shift patterns. In contrast to mammalian HOs, *Nm*HO requires only a single propionate interacting with the buried terminus of Lys16 to exhibit full activity and tolerates the existence of a propionate at the exposed 8-position. The structure of the C-terminus is qualitatively retained upon deletion of the 7-propionate but a dramatic change in the 7-propionate carboxylate ^{13}C chemical shift upon C-terminal cleavage confirms its role in the interaction with the C-terminus. The stronger hydrophobic contacts between pyrroles A and B with *Nm*HO contribute more substantially to the substrate binding free energy than in mammalian HOs, “liberating” one propionate to stabilize the C-terminus. The functional implications of the C-terminus in product release are discussed.

Heme oxygenase, HO[1], is the widely distributed enzyme (1) that utilizes hemin as both substrate and cofactor to stereospecifically cleave a single meso position to generate biliverdin, iron and CO, proceeding via the intermediates depicted in Scheme 1.

[†]This research was supported by grants from the National Institutes of Health, GM62830 (GNL), and CA132861 (KMS); NMR instrumentation purchase was supported by grants from the National Institutes of Health, RR1973, and the National Science Foundation, DBIO722538.

[*]Corresponding author: lamar@chem.ucdavis.edu, phone: 530-752-0958; FAX: 530-752-8995.

SUPPORTING INFORMATION Seven figures (uv-visible spectra, enzyme assays, five 2D NOESY spectra) and four Tables (substrate and active site residue chemical shifts for PH*IX* and DMDH*IX* derivatives); total pages 15. This material is available free of charge via the Internet at http://pubs.acs.org.

$watermark-text
$watermark-text
$watermark-text

$watermark-text

$watermark-text

$watermark-text

In mammals, the three products serve as a precursor to the powerful antioxidant bilirubin, as a source of 97% of the required iron and as a neural messenger, respectively (2-6). In plants and photosynthetic bacteria, the product open tetrapyrrole serves as a precursor to light-harvesting pigments (7), while the released iron is vital to infection for some pathogenic bacteria; (2, 4). The mammalian HOs have been the most extensively studied (3) and, in spite of only limited sequence homology (4), both the characteristic α-helical topology (8-13) and the mechanism (2, 4, 6) are conserved among other HOs. The relatively loose binding of substrate by HOs, as evidenced by both numerous vacancies and variable position of structural elements (8-13), involves an axial bond to a His, two salt-bridges between the ubiquitous propionates and two suitably positioned cationic side chains as depicted in Figure 1A; the remaining interactions are relatively weak van der Waal contacts with pyrroles A and B.

The stereoselectivity of the cleavage arises from the steric effect of the distal helix which tilts the active Fe^{3+}-OOH toward one meso position while blocking the remaining three meso positions (9-13). The particular meso position cleaved depends on the in-plane orientation of the substrate relative to the distal helix. Only the α-meso position is cleaved in mammalian HOs. The crucial role of propionate links in determining the in-plane orientation, and hence stereoselectivity, of substrate cleavage is confirmed by studies on human HO, hHO, (14) mutants where repositioning the cationic side-chains leads to a ~90° in-plane rotation of substrate with concomitant conversion of α-meso to mixed β, δ-meso cleavage. Earlier studies of human HO, hHO, with a variety of modified substrates (15, 16), have revealed that, while there is toleration for a wide range of substituents on pyrroles A and B (Figure 1B), the two propionates at positions 6 and 7 must both be conserved to retain activity.

In spite of sharing the same folding topology and mechanism with mammalian HOs, the HOs from pathogenic bacteria (2, 4-6) exhibit some distinct properties relative to function. Three pathogenic bacterial HOs have been structurally characterized, those from *Neisseria meningitidis* (9, 11), *Nm*HO, *Pseudomonas aeruginosa* (13), *Pa*HO, and *Corynbacterium diphtheria* (12), *Cd*HO. *Cd*HO, which exhibits the closest sequence and structural homology (4, 6, 12) to mammalian HOs, exhibits the same stereoselectivity, sensitivity to mutation (17), and similar 90° in-plane rotation, and altered stereoselectivity, upon mutation of cationic residues(18), as mammalian HOs (14, 19). *Pa*HO exhibits (13, 20) mixed β-,δ-meso cleavage due to an ~90° in-plane rotation of protohemin-IX relative to that in mammalian HOs, resulting from the rearrangement of cationic side chains in the wild-type protein.

*Nm*HO exhibits numerous distinct properties. While there is normal α-meso cleavage consistent with protohemin-IX oriented as depicted in Figure 1B, the structure of the active site is more compact and has fewer vacancies(9, 11) than in other HOs. The roles of the propionates in the crystal structures are not well-defined and key C-terminal residues are undetected (9, 11). In contrast, solution NMR has demonstrated that the C-terminal fragment, His207Arg208His209, is, in fact, ordered and interacts with the active site (21-24). A molecular model based on limited energy minimization and using as constraints limited NOESY data and a series of proposed salt bridges suggested by the crystal structure, has been offered (22, 24) and is reproduced in Figure 2. We note that this model utilizes one of the two propionates (at native PH*IX* position 7 in the crystal (9, 11)), leaving but one propionate to make the conventional salt bridge to the protein matrix. Surprisingly, the *Nm*HO C-terminus cleaves spontaneously upon substrate binding (22) to yield a complex with an increased rate of product release. The fact that the necessary acceleration of product release (25) in mammalian HOs occurs (3) by the binding of biliverdin reductase, BVR, at the exposed substrate site(26) that is homologous to the site of the C-terminal interaction in *Nm*HO, demands a more quantitative understanding of the C-terminus in the latter complex.

$watermark-text

$watermark-text

$watermark-text

We have pursued detailed ^{1}H NMR studies (21-24, 27)of systematically perturbed interactions of the substrate with *Nm*HO in general, and its C-terminal fragment in particular, to evaluate the molecular model (Figure 2) and ascertain the structural features that favor the facile cleavage of the C-terminus. Studies of the three sequential C-terminal deletion mutants directly confirmed (24) the substrate contacts to His207 and Arg208 and indicated the existence of a salt bridge for the C-terminal carboxylate with a cationic side chain of both Arg208 and Lys126. Systematic variation of substrate pyrroles A/B substituents revealed (27) a much tighter interaction between substrate and protein matrix, and hence much stronger descrimination between the alternate substrate orientation about the α,γ-meso axis, than in any other HO (20, 28-30), and that the C-terminal cleavage rate increased (24) as the pyrrole A substituent size decreased. Herein we complete these studies by perturbing the substrate propionates, both by replacement of individual propionates by methyls, as well as by interchanging methyl and propionate on one pyrrole, in order to ascertain whether the propionates must be conserved for activity, as found in mammalian HOs (15, 16), and identify the interactions of the propionates at each position.

To this end, we take advantage of a series of modified hemins (31, 32) depicted in Figure 3 designed to illuminate the interaction of substrates with *Nm*HO relative to that in mammalian HOs; labeling of these substrates is based on modifications of protohemin-IX (PH*IX*) and 2-4-dimethyldeuterohemin-IX (DMDH*IX*). We emphasize the low-spin azide complex where the novel orbital ground state (33) results in strongly contact-shifted, and hence resolved, signals (24, 27, 34, 35) for the protons on the substrate edge exposed to solvent which makes contact to the C-terminus (see Figure 2). While relaxation for the azide complexes is somewhat stronger for the more frequently studied cyanide complexes (36), it does not seriously interfere with effective 2D NMR analysis (24, 27, 35), and the physiological oxy-complex is more reasonably modeled by the bent azide than the linear cyanide ligand.

MATERIAL AND METHODS

Materials

The wild type, WT, *Neisseria meningitidis* heme oxygenase, *Nm*HO, was prepared and purified as described in detail previously (21). The two derivatives of protohemin-IX with selective methyl for propionate substitutions, 6-de-propionate-,6-methyl-protohemin-IX, and 7-de-propionate-,7-methyl-protohemin-IX, labeled (6P→M)PH*IX* and (7P→M)PH*IX*, 2-,4-dimethyldeuteroheme-IX, DMDH*IX*, and protohemin-XIII, PH*XIII*, (which possesses the symmetric 1-,4-divinyl arrangement) are the same as described in detail previously (32). The two hemins with selective removal or rearrangement of propionates, based on 2-,4-dimethyldeuterohemin-IX (labeled DMDH*IX*, are 7-de-propionate-,7-methyl-2-,4-dimethyldeuterohemin-IX, labeled (7P→M)DMDH*IX*, and 7-de-propionate-,7-methyl-,8-de-methy,8-propionate-2-,4-dimethyldeuterohemin-IX, labeled (7P→M:-8M→P)DMDH*IX*, which were prepared as described elsewhere (31). The positions on the DMDH*IX* and PH*XIII* derivatives are labeled (see Figure 3) on the basis of the orientation of native protohemin-IX in the crystal structure, as shown in Figure 1B (9, 11). The carboxylates of native protohemin-IX were 95% ^{13}C-labeled singly or doubly to yield 6-($^{13}C_\gamma O^-_2$)PH*IX* and 6,7-($^{13}C_\gamma O^-_2)_2$PH*IX*, respectively, as described elsewhere (37).

The 1:1 complexes of the substrate of interest with *Nm*HO were prepared as described previously (21) for the PH*IX* and DMDH*IX* complexes, except that the mono-propionate hemins were dissolved in 95% H_2O, 5% pyridine, with the pyridine removed immediately after preparation via Sephadex column chromatography, as described previously for the reaction with globins (38). The quantitative incorporation of each substrate into *Nm*HO was confirmed both by the characteristic uv-visible spectra as the cyanide complexes and the

identification of the signals in the ^{1}H NMR spectrum as the azide complexes. Samples for ^{1}H NMR were concentrated by ultrafiltration to yield ~2mM samples in 50 mM phosphate, 75 mM azide, pH ~7.1.

UV-visible spectroscopy

Spectra were recorded on a Varian Cary 50 uv-visible spectrometer over the range 200-800nm at a rate of 50 nm/s; 32 transients were averaged. The sample *Nm*HO substrate complexes were 30 mM in cyanide 50 mM in phosphate, pH 7.1.

In vitro enzyme assay

The activity of the various substrate complexes of *Nm*HO was determined by following by uv-visible spectroscopy the effect of reaction with ascorbate, in the presence of the iron chelator desferrioxamine, in the conversion of hemin to biliverdin, as described in detail previously (21). Subsequently, the product biliverdin was reacted with rat biliverdin reductase, prepared as described elsewhere (39), and NADPH to generate bilirubin.

NMR spectroscopy

^{1}H NMR data were collected on Bruker AVANCE 500 and 600 spectrometers operating at 500 and 600 MHz, respectively. ^{1}H chemical shifts are referenced to 2,2-dimethyl-2-silapentane-5-sulfonate (DSS) through the water resonance calibrated at each temperature. Reference spectra were collected over a 65 ppm spectral width and a repetition rate 2.5 s^{-1}. 600 MHz NOESY spectra (40) (mixing time 40 ms; repetition rate 1.5 to 2.5 s^{-1}) and 500 MHz Clean-TOCSY spectra (41) (to suppress ROESY response; 25°, 35°C, spin lock 25 ms; repetition rate 1-2 s^{-1}) were recorded over a bandwidth of 20 and 45 ppm (NOESY) and 20 ppm (TOCSY) using 512 t1 blocks of 128 and 256 scans each consisting of 2048 t2 points. 2D data sets were apodized by 30°- or 45°-sine-squared-bell-functions and zero-filled to 2048 × 2048 data points prior to Fourier transformation.

^{1}H-decoupled ^{13}C NMR spectra were recorded at 125 MHz on a Bruker AVANCE 500 spectrometer over a bandwidth 300 ppm at the repetition rate of 1 s^{-1} at 25° C utilizing 32K data points. The ^{13}C chemical shifts were indirectly referenced to the proton spectrum (42).

RESULTS

Structural integrity of propionate-modified substrate complexes

The reaction of (6P→M)PH*IX* and (7P→M)PH*IX* with *Nm*HO, in the presence of excess cyanide resulted in the same characteristic changes in their uv-visible spectra as observed for native PH*IX*, while reaction of (7P→M)DMDH*IX* and (7P→M:8M→P)DMDH*IX* with *Nm*HO in the presence of excess cyanide resulted in the same uv-visible spectral changes as observed for the DMDH*IX* complex (Supporting Information Figure S1). The near identity of the uv-visible spectra of the *Nm*HO complexes with the propionate modified and "normal" dipropionate substrates support the incorporation of the modified substrate into an environment that is essentially the same as that for PH*IX* and DMDH*IX*. The ^{1}H NMR spectra of the azide complexes of (7P→M)PH*IX* and (6P→M)PH*IX* are presented in Figures 4B and 4C, respectively, where they can be compared with that of the complex with native PH*IX* (Figure 4A). Also included is the ^{1}H NMR spectrum of the azide complex for the two-fold symmetric PH*XIII* (Figure 4D). The NMR spectra of the *Nm*HO azide complexes of (7P→M)DMDH*IX* and (7P→M:8M→P)DMDH*IX* are shown in Figures 5B and 5C, respectively, and can be compared with that of the previously characterized DMDH*IX* complex (24) shown in Figure 5A. The NMR spectra in Figures 4B, 4C, 4D, 5B and 5C display a strongly dominant single set of hyperfine shifted methyl signals which

$watermark-text $watermark-text $watermark-text

indicate an unique orientation of the modified substrates within an active site very similar to that observed for the “normal” dipropionate PH*IX* and DMDH*IX*.

Activity of modified substrate complexes

The complexes with modified substrates all underwent reaction with ascorbate in the presence of the iron chelator, desferrioxamine, in a standard assay (22) that yielded uv-visible spectra with characteristic broad bands at ~380 and ~670 nm (43) indicative of biliverdin formation, with the resulting spectra largely indistinguishable from those of the related substrates with the two normal propionates (Supporting Information Figure S2). Subsequent reaction of the biliverdin with rat biliverdin reductase (39) and NADPH afforded the spectra indicative of bilirubin formation. Thus, HO activity is conserved upon either deletion of one propionate or exchange between a propionate and methyl on the same pyrrole.

Substrate/active site residue assignment protocols

Substrate protons for the major isomers in solution are labeled $M_i(H_i)$ for methyl (single proton) at pyrrole positions i=1-8 (see Figure 1). Residue protons are labeled by residue number and position; peptide protons are labeled only by position. Unambiguous assignment of the substrate resonances is obtained by characteristic NOESY connectivities about the periphery and is facilitated by the expected pattern of substrate hyperfine shifts (24, 27, 35). On the one hand, cross peaks between a pair of methyls on the same pyrrole (adjacent to a common meso position) are strong (weak). Methyl to vinyl H_βs (H_αs) NOESY cross peaks are strong for a vinyl oriented *cis* (*trans*) to its adjacent methyl (27) as depicted in Figure 3. On the other hand, the known orbital ground state for the azide complex places large τ spin-density (24, 27, 34, 35)only at positions 1, 4, 5 and 8, such that methyl and vinyl H_αs appear strongly shifted to low field, with the vinyl H_βs exhibit strongly upfield shifted and resolved resonances. Substrate chemical shifts for pyrrole α-substituents are listed in Table 1; complete substrate assignments and active site residue assignments are provided in Supporting Information, Tables S1, S2 and S3, S4.

Active site residues are assigned sequence-specifically (44) by characteristic backbone NOESY cross peaks among TOCSY-detected residues characteristic of an α-helix (data not shown) as described in detail previously for a series of *Nm*HO and hHO azide complexes (24, 27, 35). These studies afford the assignments for the helical fragments; proximal helix Thr19-Val26, Phe52-Lys54, distal helix Tyr112-Gly116, Phe123-Phe125, Arg140-Leu142 and Ala180-Tyr184. The two residues focal to establishing the orientation of a substrate in the active site (27) are Phe123 in contact with substituents at positions 1 and 8, and Cys113 in contact with substituents at positions 4 and 5 in the crystal structure (Figure 1B). Chemical shifts for the axial His23 are included in Table 1 and for other residues are provided Supporting Information, Tables S3 and S4.

Seating of propionate-modified substrates

To uniquely place modified substrates in the active site of *Nm*HO we will describe the proton at a given position on the modified substrate, as labeled in Figure 3, and identify where each of those protons on the substrate is placed in the active site defined by the position of the PH proton in the crystal structure, as shown in Figure 1B (9, 11). Portions of the ^{1}H NMR NOESY spectrum of *Nm*HO-(7P→M)PH*IX*-N_3 for assigning the substrate and active site residues relevant to substrate seating are shown in Figure 6. A weak cross peak between two low-field methyls (Figure 6B) locates the M_1/M_8 pair, and an intense cross peak of one of these to a more weakly low-field shifted methyl (Figure 6H) identifies the M_8/M_7 pair. Intense cross peaks of high-field resolved vinyl H_βs to a partially resolved methyl and a strongly low-field shifted H_α locate the 4-vinyl group and M_3 (not shown).

$watermark-text

$watermark-text

$watermark-text

The remaining low-field methyl exhibits cross peaks to a moderately low-field shifted pair of H αs and H_{β}s that identify the 5-methyl and 6-propionate. The M_1 cross peaks to another vinyl H βs locate the 2-vinyl group and establish that both vinyl groups are oriented *cis*, as in the crystal structure (9, 11)for the PH*IX* complexes, as shown in Figure 3B. The M_1 and M_8 cross peaks to Phe123 and the M_5 (and 4-vinyl; not shown) cross peak to Cys113 $C_{\alpha}H$ (Figure 6A) establish an orientation where the lone propionate is in the position of the 6-propionate in the crystal structure (Figure 1B). M_1/M_8 contacts to two residues not predicted by the crystal structure are observed to both the ring $C_{\delta}H$ (Figure 6I) and $C_{\beta}H_2$ (Figure 6A) of a His and the $C_{\alpha}H$ (Figure 6B) of another residue, in a fashion very similar to that observed in PH*IX* and DMDH*IX* complexes (24, 35). The molecular model and C-terminal deletions have shown (24) that these contacts involve His207 and the $C_{\alpha}H$ of Arg208.

The reference spectrum for *Nm*HO-(6P→M)PH*IX*-N_3 exhibits somewhat broader peaks than the other complexes but still allows the necessary assignments (Supporting Information Figure S3). The weak, resolved intermethyl cross peak that identifies M_1/M_8 and their cross peaks to the Cys113 $C_{\alpha}H$ demonstrate that the orientation of the substrate is rotated 180° about the α,γ-meso position relative to native PH*IX* in the crystal (as shown in Figure 3B). Strongly upfield shifted vinyl H_{β}s exhibit weak cross peaks to the remaining low-field methyl and to the vinyl H_{α}, which in turn, exhibits a cross peak to a partially resolved methyl, identifying M_5, M_3 and the 4-vinyl in the *trans* orientation (as shown in Figure 3C). A cross peak from M_1 to a vinyl H α shows that the 2-vinyl is similarly in the *trans* orientation (as depicted in Figure 3B). M_5 in the 180°-rotated orientation exhibits cross peaks to a His $C_{\beta}H_2$ and the $C_{\alpha}H$ of another residue that dictates their origin as His207 and Arg208.

The NOESY spectrum of *Nm*HO-(7P→M)DMDH*IX*-N_3 (Supporting Information Figure S4) locates three pairs of strongly coupled methyls with weak coupling between the pairs, and another weak coupling to a seventh methyl that uniquely identify M_1-M_5 and M_7, M_8. The M_5 contacts to C_{β}Hs locates the 6-propionate. The M_1/M_8 cross peaks to Phe123 and the M_5/M_4 cross peaks to Cys113 uniquely determine the orientation where the lone propionate occupies the same position as does the 6-propionate in the crystal structure (Figure 3E). The M_8/M_1 exhibit NOESY cross peaks to both the C_{β}Hs and $C_{\delta}H$ of a His and the $C_{\alpha}H$ of another residue that identify His207 and Arg208. It is noted that M_8 contacts occur to both the backbone and ring of His207; this latter contact was much weaker or undetected in the complexes with the native PH*IX* (or DMDH*IX*) possessing the normal propionates at both positions 6 and 7.

The NOESY spectrum of *Nm*HO-(7P→M:8M→P)DMDH*IX*-N_3 depicts two pairs of strongly coupled methyls which collectively identify the pairs M_1/M_2 and M_3/M_4. A weak cross peak between the pairs, as well as a weak NOE from one of the pairs to a low-field methyl, identifies M_1-M_5; the M_5 contacts to a $C_{\alpha}H$ locate the 6-propionate (Supporting Information Figure S5). A less-strongly low-field shifted methyl exhibits cross peaks to a low-field shifted C αH and C_{β}Hs of a propionate identifying the remaining M_7 and 8-propionate; $H_{8\alpha}$ exhibits a weak cross peak to M_1. Contacts of M_1/M_8 with Phe123 and M_4/M_5 with Cys113 establish the orientation with one propionate occupying the crystallographic 6-propionate position and the other in the crystallographic 8-positions (as depicted in Figure 3F). The contact of $H_{8\alpha}$ to a $C_{\alpha}H$ of one residue, and $M_1/H_{8\alpha}$ contacts to the C_{β}Hs of an apparent His, represent the interaction of His207 and Arg208 with the active site. It was not possible to locate the His207 $C_{\delta}H$, but M_1 and $H_{8\alpha}$ cross peaks to C_{β}Hs not predicted by the crystal structure indicate their origin as His207.

The NOESY spectrum of *Nm*HO-PH*XIII*-N_3 (not shown) identifies all the substrate signals with the NOESY cross peak of the 1-vinyl $H_{1\beta}$ to M_8 and Phe123 and $H_{1\alpha}$ cross peak to M_2,

indicating that the vinyl group is in a *trans* position (as depicted in Figure 3C). The 4-vinyl group exhibits the same cross peaks as in PH*IX* and hence retains the conventional *cis* orientation. The $M_8/H_{1\beta}$ cross peaks to a $C_\beta H_2$ group and the M_8 cross peak to a $C_\alpha H$ locate His207 and Arg208. All chemical shift data are provided in Supporting Information, Tables S1 and S3.

Loss of substrate-residue contacts upon NmHO "aging"

Over a period of a few days at 25°C, the resolved resonances of the WT *Nm*HO complexes with (7P→M)PH*IX*, (7P→M)DMDH*IX* and (7P→M:8M→P)DMDH*IX* disappear and are replaced in the conversion to an "aged", or homogeneously degraded, derivative which we label *Nm*HO^X. The reference spectra for the three "aged" derivatives are illustrated in Figure 4B' and Figures 5B' and 5C', respectively. Concomitant to the generation of *Nm*HO^X are observed the appearance of two very narrow resonances in the aromatic spectral window. Similar conversion of *Nm*HO to *Nm*HO^X has been characterized in detail for both PH*IX* and DMDH*IX* complexes and the product shown (21, 22) to be the result of cleavage of the Arg208His209 dipeptide. In contrast, the WT *Nm*HO complexes of (5P→M)PH*IX* and PH*XIII* exhibit only minor (<10%) "aging" over the same period of time, dictating that the terminal cleavage rate must be significantly (factor >10) slower relative to that for either the other propionate modified or native PH*IX* and DMDH*IX* substrates. Unfortunately, the very sparingly available complexes of the propionate-modified substrates were heterogeneously decomposed upon completion of 2D NMR, precluding meaningful mass spectrometric studies to characterize the initially cleaved peptide.

The NOESY spectrum of *Nm*HO^X-(7P→M)PH*IX*-N_3 provides the same assignment as for the WT *Nm*HO complex (not shown). The most prominent difference is that the M_1/M_8 contacts to the His207 and Arg208 are lost (see Figure 6A'). Similar NOESY data for the *Nm*HO^X complexes of (7P→M)DMDH*IX* and (7P→M:8M→P)DMDH*IX* (Supporting Information Figures S6 and S7, respectively), in each case, exhibit a largely conserved active site structure but with the loss of the M_1/M_8 and $M_1/H_{1\alpha}$ contacts to His207 and Arg208. The loss of these contacts is consistent with cleavage of the C-terminus. The substrate chemical shifts are perturbed upon "aging" in a manner close to that observed (21, 23) for PH*IX* and DMDH*IX*. Active site residues chemical shifts are only inconsequentially perturbed by "aging". Both substrate (Tables S1, S2) and active site residue (Tables S3, S4) chemical shifts for the *Nm*HO^X complexes are provided in Supporting Information.

Effect of C-terminal cleavage on the substrate propionate carboxylates

The conversion of native *Nm*HO–PH*IX*-H O to yield *Nm*HO^X 2 -PH*IX*-H_2O by the loss of Arg208His209 is relatively rapid (half life 24 h) and is readily followed (22) by ^1H NMR via the relative intensities of the resolved M_8 peaks. Figure 7A provides the ^{13}C NMR spectrum in the carboxylate spectral window for *Nm*HO-(6,7-$^{13}CO^-_2$)$_2$PH*IX*-H_2O (~90% *Nm*HO and ~10% *Nm*HO^X), which reveals two well-spaced signals, labeled *a* and *b*, uniquely attributable to the two labeled carboxylates. The spectrum of this complex upon ~25% degradation to *Nm*HO^X is shown in Figure 7B and identifies the degraded species with peaks labeled *c* and *d*; clearly the chemical shift for one propionate is conserved upon C-terminal cleavage while the other one significantly perturbed. The ^{13}C NMR spectrum of a partially degraded, singly labeled complex, *Nm*HO-(6-$^{13}CO^-_2$)PH*IX*-H_2O (~75% *Nm*HO, ~25% *Nm*HO^X), is shown in Figure 7C and confirms that the propionate sensitive to C-terminal cleavage is clearly that at the crystallographic 7 position.

$watermark-text $watermark-text $watermark-text

$watermark-text

$watermark-text

$watermark-text

DISCUSSION

Structure of the active site

Both uv-visible and ^{1}H NMR spectroscopy clearly show that each of the propionate-modified substrates quantitatively incorporate into the active site of *Nm*HO; standard *in vitro* assays (22) show that the complexes retain full activity. The ^{1}H NMR data establish that the substrates seat overwhelmingly in a single orientation that in each case dictates that the only propionate protein salt-bridge crucial to substrate binding to *Nm*HO is that between Lys16 with the 6-propionate position in the crystal structure (9, 11). The strong conservation of active site structure, in spite of the drastic propionate deletion/rearrangement, is confirmed by not only the conserved pattern of NOESY cross peaks, but also by the conservation of the pattern of hyperfine shifts. On the one hand, non-ligated active site residues exhibit only dipolar shifts (36, 45) which sensitively reflect the anisotropy/orientation of the paramagnetic susceptibility tensor, χ, and the position of the residue. Even small changes in the orientation of χ can result in large changes in the dipolar shift pattern (23, 46). The dipolar shifts for crystallographically detected active site residues are highly conserved among the variable substrates and upon C-terminal cleavage (Supporting Information Tables S3 and S4) dictating that both the orientation of χ and the residue geometries are conserved among the complexes.

On the other hand, ligated His23 and substrate hyperfine shifts are dominated by the contact interaction (36, 45) (and to a lesser degree, by 2,4-substituents) (47). The data in Table 1 show that the pattern of the His23 C_βHs, and hence the orientation of the His imidazole relative to the protein matrix, is conserved for the various substituents. Substrate methyls very sensitively reflects the in-plane rotational orientation of the substrate relative to the axial histidine imidazole plane(36, 48), and by inference, the protein matrix. Thus the pattern of the M_1, M_3, M_5 and M_8 shifts is inconsequentially differentiated within the pair of complexes of PH*IX* and (7P→M)PH*IX*-N_3 (see Table 1); the same highly conserved pattern of M_1, M_2, M_3, M_4 and M_5 shift pattern is observed within the three complexes of DMDH*IX*, (7P→M)DMDH*IX*-N_3 and (7P→M:8M→P)DMDH*IX*. For the (6P→M)PH*IX* complex with the "reversed" orientation (Figure 3B), the pattern of methyl shifts is conserved relative to that for the equilibrium ~20% populated "reversed" orientation (27) of native PH*IX* (data in column 2 of Table 1). This dictates that the in-plane orientation of the substrate is inconsequentially affected by either deletion or rearrangement of one of the propionates. Lastly, the low-field bias for H-bond signals for Gln49 and His53, which are linked to the axial ligand via the catalytic water molecules (9, 11), is strictly conserved.

Structure of the C-terminus and its cleavage

Each of the *Nm*HO complexes of these propionate-modified substrates exhibit contacts to residues at the crystallographically exposed 1 and 8 positions, (*i.e.*, the positions of the PH*IX* 1CH_3 and CH_3 in the crystal structure; Figure 1B) that are not described in the crystal structure in which the C-terminal His207Arg208His209 fragment is undetected (9, 11). This absence in the crystal was attributed to structural disorder, but possible loss of the C-terminus by an unusual degradation clearly established in solution by ^{1}H NMR and mass spectrometry(22), has not been yet ruled out. In any case, these contacts have been assigned to His207 and Arg208, and were confirmed by C-terminal deletion (22). A molecular model (24) based on limited energy minimization using NOESY constraints and a series of three salt bridges and one H-bond involving the three C-terminal residues, the side chain of Lys126, the carboxylate of Asp27 and the propionate at the crystallographic 7-position, is reproduced in Figure 2. The observation of very similar His207 and Arg208 interactions with the active site with each of the modified substrates indicates that the architecture of the

$watermark-text

$watermark-text

$watermark-text

interaction of the C-terminus with the active site is qualitatively retained upon loss of the 7-propionate to Arg208 salt bridge.

The relatively modest effect on the C-terminal structure upon deleting the 7 propionate could be attributed to the failure of the 7 propionate to interact with the C-terminus, as described by our model (22, 24). However, the ^{13}C chemical shift for the PH*IX* propionate carboxylates (Figure 7) is strongly perturbed for the 7 propionate, but not for the 6 propionate, upon C-terminal cleavage, confirming that the 7 propionate does interact with the C-terminus in the native complex. The loss of the 7 propionate salt bridge may weaken, but not significantly rupture, the interaction of the C-terminus with the active site. This confirms the relatively robust nature of this interaction of the C-terminus with the active site (24). Qualitative changes upon deleting the 7 propionate include slightly altered hyperfine shifts for His207 in spite of conserved χ, and more intense NOESY cross peaks between $8CH_3$ and the His207 $C_\delta H$ than in complexes with the native propionates. Inasmuch as the C-terminal interaction with the active site in 7-propionate deleted substrates is not biologically relevant, no attempt was made to model this interaction.

It is not clear whether the propionate at the crystallographic 8-position in *Nm*HO-(7P→M:8M→P)DMDH*IX*-N_3 interacts with the terminus of Arg208. The molecular model suggests that the carboxylate of the 8-propionate could orient to form the salt bridge. The fact that the C-terminal cleavage leads to significant chemical shift changes for the 8-propionate $C_\beta H$ chemical shifts (−1.50, −0.80 in WT *Nm*HO to −0.80, −0.49 in *Nm*HO^X) suggests that a salt bridge between the 8 propionate and Arg208 side chain may occur in this complex.

NMR studies (22, 24) with variably 2-,4-disubstituted substrates had shown that the rate of C-terminal cleavage correlates with the proximity of the His207 to the substrate, with the rate of cleavage significantly enhanced upon replacing the bulky vinyls with methyls or hydrogens. Both (6P→M)PH*IX* and PH*XIII* have the vinyl at the crystallographic 1 position oriented *trans* (H_βs close to position 8; see Figures 3B and 3C), which will sterically interfere with His207 approaching the substrate. The retarded rates of cleavage for these two modified substrates are consistent with its model.

Comparison to other HOs and functional implications

Clearly *Nm*HO requires but a single propionate salt bridge to the protein matrix to effectively bind substrate, in contrast to mammalian HO (15, 16). Moreover, protohemin-I (the analog to (7P→M:8M→P)PH*IX*, but with 2,4-vinyls) fails to yield an active hHO complex (15). In contrast, the (7P→M:8M→P)PH*IX* complex (Figure 3F) retains full activity in *Nm*HO. The fact that deleting one propionate abolishes substrate binding for hHO but not *Nm*HO dictates that other substrate-enzyme interactions must be stronger in the *Nm*HO than hHO complex. Since one salt bridge between the propionate at position 6 (Figure 1) with the side chain terminus of a Lys (Lys16 for *Nm*HO, Lys18 for hHO) is conserved, it is reasonable to attribute the stronger interactions in *Nm*HO to van der Waals contacts primarily with pyrroles A and B. Stronger van der Waals interactions have been implied in the much more compact active site in crystals (2, 9, 11). A similar conclusion has been reached on the basis of the much stronger orientational preference of substrates about the α-, γ-meso axis (27) when compared to other HOs (20, 28-30). Hence, the stronger substrate-enzyme van der Waals interactions in *Nm*HO substrate complexes can be viewed as a mechanism for “liberating” one of the two propionates for a functional role unnecessary in other HOs, namely the ordering of the C-terminus to interact with the active site.

The solution NMR-detected C-terminal interaction with the active site can be expected to have functional implications for two distinct processes that most likely occur at the exposed substrate edge that, in *Nm*HO, is “shielded” by the interaction of the C-terminus with the

$watermark-text

$watermark-text

$watermark-text

active site (24). On the one hand, HO-biliverdin complexes dissociate too slowly to sustain effective biological catalysis (25). For mammalian systems the product biliverdin is not released until a transient 1:1 complex is formed with BVR with contact at the exposed substrate edge (26). The BVR acts as a cooperative facilitator that significantly accelerates the rate of biliverdin release and at the same time precludes the presence of significant concentrations of the toxic biliverdin. While bilirubin may not be toxic for bacteria, there is still the need for the transient binding of an allosteric effector (the BVR analog) to accelerate biliverdin release. On the other hand, while cytochrome-P450 reductase and NADPH or ascorbate react with mammalian systems directly to yield iron-free biliverdin (3), the same reactions with *Nm*HO complexes proceed only to the iron (III)-biliverdin complex where the iron can only be extracted by a powerful iron chelator (2, 49). The final reduction step for *Nm*HO complexes must rely on the specific *Nm*HO electron donor. It is possible, that once the iron biliverdin complex of *Nm*HO is formed, the native electron donor protein may serve as both a source of the key electron for the iron as well as an allosteric effector to labilize the resulting iron-free biliverdin. Unfortunately, neither the BVR analog nor the electron donor in pathogenic bacteria is known (2). A more detailed understanding of the fate of biliverdin in *N. meningitidis* would be necessary to provide fruitful insight into the unique C-terminal structural role of *Nm*HO.

CONCLUSIONS

*Nm*HO binds substrates possessing a single propionate to form active complexes by either deleting or rearranging the position of one of the propionates of the substrate. This is in strong contrast with hHO where neither the propionate deletion nor rearrangement affords and active complex. The unique salt bridge for *Nm*HO is between the propionate at the crystallographic 6 position and the terminus of Lys16. The second substrate propionate at the normal crystallographic 7 position (and possibly at the unprecedented 8 position), forms a salt bridge to the (crystallographically undetected) side chain of Arg208 as a portion of the stabilization of the interactions of the C-terminus with the active site. The solvent-exposed side of the substrate consisting of the crystallographic 1 and 8 positions interacts with the C-terminus in a qualitative conserved manner upon elimination of the 7-propionate, as described by an earlier molecular model (24), although altered hyperfine shifts suggest some minor rearrangement in the C-terminus architecture. Spontaneous C-terminal cleavage abolishes the characteristic contacts between the C-terminus and active site with the exception for substrates oriented with the vinyl group at the crystallographic 1 position, which interferes with the interaction of the C-terminus with the active site. The effective binding of a substrate with a single propionate by *Nm*HO, instead of the required two from mammalian HOs, is attributed to a larger contribution to the substrate binding from peripheral van der Waals interactions, as supported by more compact structure (2, 9, 11), fewer vacancies and much stronger orientational preference about the α,γ-meso axis (27). These structural differences are proposed to have evolved, in part, to “liberate” one propionate for stabilizing interactions of the active site with the C-terminus, which, in turn, is proposed to function in product release.

Supplementary Material

Refer to Web version on PubMed Central for supplementary material.

Abbreviations used

BVR	biliverdin reductase
DSS	2,2-dimethyl-2-silapentane-5-sulfonate

$watermark-text

$watermark-text

$watermark-text

HO	heme oxygenase
hHO	human heme oxygenase-1
***Nm*HO**	*Neisseria meningitidis* heme oxygenase
***Cd*HO**	*Corynebacterium diphtheriae* heme oxygenase
***Pa*HO**	*Pseudomonas aeruginosa* heme oxygenase
NOESY	two-dimensional nuclear Overhauser spectroscopy
TOCSY	two-dimensional total correlation spectroscopy
ROESY	rotating-frame two-dimensional Overhauser spectroscopy
PH*IX*	protohemin-IX
PH*XIII*	protohemin-XIII
DMDH*IX*	2-,4-dimethyldeuterohemin-IX
(6P→M)PH*IX*	6-de-propionate-,6-methyl-protohemin-IX
(7P→M)PH*IX*	7-de-propionate-,7-methyl-protohemin-IX
(7P→M)DMDH*IX*	7-de-propionate-,7-methyl-2-,4-dimethyldeuterohemin-IX
(7P→M: 8M→P)DMDH*IX*	7-de-propionate-,7-methyl,8-de-methyl,8-propionate-2-,4-dimethyldeuterohemin-IX

REFERENCES

1. Tenhunen R, Marver HS, Schmid R. Microsomal heme oxygenase. Characterization of the enzyme. J. Biol. Chem. 1969; 244:6388–6394. [PubMed: 4390967]
2. Wilks A. Heme Oxygenase: Evolution, Structure, and Mechanism. Antioxidants Redox Signal. 2002; 4:603–614.
3. Ortiz de Montellano, PR.; Auclair, K. Heme Oxygenase Structure and Mechanism. In: Kadish, KM.; Smith, KM.; Guilard, R., editors. The Porphryin Handbook. Elsevier Science; San Diego, CA: 2003. p. 175-202.
4. Frankenberg-Dinkel N. Bacterial Heme Oxygenases. Antoxidants Redox Signal. 2004; 6:825–834.
5. Rivera M, Zeng Y. Heme Oxygenase, steering dioxygen activation toward heme hydroxylation. J. Inorg. Biochem. 2005; 99:337–354. [PubMed: 15598511]
6. Unno M, Matsui T, Ikeda-Saito M. Structure and catalytic mechanism of heme oxygenase. Nat. Prod. Rep. 2007; 24:553–570. [PubMed: 17534530]
7. Beale SI. Biosynthesis of open-chain tetrapyrroles in plants, algae, and cyanobacteria. Ciba Foundation Symposium. 1994; 180:156–168. [PubMed: 7842851]
8. Schuller DJ, Wilks A, Ortiz de Montellano PR, Poulos TL. Crystal structure of human heme oxygenase-1. Nature Struct. Biol. 1999; 6:860–867. [PubMed: 10467099]
9. Schuller DJ, Zhu W, Stojiljkovic I, Wilks A, Poulos TL. Crystal structure of heme oxygenase from the Gram-negative pathogen *Neisseria meningitidis* and a comparison with mammalian heme oxygeanse-1. Biochemistry. 2001; 40:11552–11558. [PubMed: 11560504]
10. Sugishima M, Sakamoto H, Higashimoto Y, Omata Y, Hayashi S, Noguchi M, Fukuyama K. Crystal structure of rat heme oxygenase-1 in complex with heme bound to azide: Implication for regiospecific hydroxylation of heme at the α-*meso* carbon. J. Biol. Chem. 2002:45086–45090. [PubMed: 12235152]
11. Friedman JM, Lad L, Deshmukh R, Li HY, Wilks A, Poulos TL. Crystal structures of the NO- and CO-bound heme oxygenase from *Neisseriae meningitidis* - Implications for O_2 activation. J. Biol. Chem. 2003; 278:34654–34659. [PubMed: 12819228]

$watermark-text

$watermark-text

$watermark-text

12. Unno M, Matsui T, Chu GC, Coutoure M, Yoshida T, Rousseau DL, Olson JS, Ikeda-Saito M. Crystal Structure of the Dioxygen-bound Heme Oxygenase from *Corynebacterium diphtheriae*. J. Biol. Chem. 2004; 279:21055–21061. [PubMed: 14966119]
13. Friedman J, Lad L, Li H, Wilks A, Poulos TL. Structural Basis for Novel δ-Regioselective Heme Oxygenation in the Opportunistic Pathogen *Pseudomonas aeruginosa*. Biochemistry. 2004; 43:5239–5245. [PubMed: 15122889]
14. Wang J, Evans JP, Ogura H, La Mar GN, Ortiz de Montellano PR. Alteration of the Regiospecificity of Human Heme Oxygenase-1 by Unseating of the Heme but not Disruption of the Distal Hydrogen Bonding Network. Biochemistry. 2006; 45:61–73. [PubMed: 16388581]
15. Frydman RB, Tomaro ML, Buldain G, Awruch J, Diaz L, Frydman B. Specificity of heme oxygenase: A study with synthetic hemins. Biochemistry. 1981; 20:5177–5182. [PubMed: 6895313]
16. Tomaro ML, Frydman SB, Frydman B, Pandey RK, Smith KM. The Oxidation of Hemins by Microsomal Heme Oxygenase: Structural Requirements for the Retention of Substrate Activity. Biochim. Biophys. Acta. 1984; 791:342–349. [PubMed: 6549143]
17. Matsui T, Furukawa M, Unno M, Tomita T, Ikeda-Saito M. Roles of Distal Asp in Heme Oxygenase from *Corynebacterium diphtheriae*. HmuO, J. Biol. Chem. 2005; 280:2981–2989.
18. Zeng Y, Deshmukh R, Caignan GA, Bunce RA, Rivera M, Wilks A. Mixed Regioselectivity in the Arg-177 Mutants of *Corynebacterium diphtheriae* Heme Oxygenase as a Consequence of in-Plane Heme Disorder. Biochemistry. 2004; 43:5222–5238. [PubMed: 15122888]
19. Koenigs Lightning L, Huang H-W, Moënne-Loccoz P, Loehr TM, Schuller DJ, Poulos TL, Ortiz de Montellano PR. Disruption of an active site hydrogen bond converts human heme oxygenase-1 into a peroxidase. J. Biol. Chem. 2001; 276:10612–10619. [PubMed: 11121422]
20. Caignan GA, Deshmukh R, Wilks A, Zeng Y, Huang H.-w. Moenne-Loccoz P, Bunce RA, Eastman MA, Rivera M. Oxidation of heme to β- and δ-biliverdin by *Pseudomonas aeruginosa* Heme Oxygenase as a Consequence of an Unusual Seating of the Heme. J. Am. Chem. Soc. 2002; 124:14879–14892. [PubMed: 12475329]
21. Liu Y, Zhang X, Yoshida T, La Mar GN. ^{1}H NMR characterization of the solution active site structure of substrate-bound, cyanide-inhibited heme oxygenase from *Neisseria meningitidis*; Comparison to crystal structures. Biochemistry. 2004; 43:10112–10126. [PubMed: 15287739]
22. Liu Y, Ma L-H, Satterlee JD, Zhang X, Yoshida T, La Mar GN. Characterization of the spontaneous “aging” of the heme oxygenase from the pathological bacterium *Neisseria meningitidis* via cleavage of the C-terminus in contact with the substrate; Implications for functional studies and the crystal structure. Biochemistry. 2006; 45:3875–3886. [PubMed: 16548515]
23. Liu Y, Ma L-H, Zhang X, Yoshida T, Satterlee JD, La Mar GN. ^{1}H NMR study of the influence of hemin vinyl-methyl substitution on the interaction between the C-terminus and substrate and the “aging” of the heme oxygenase from *N. meningitidis*. Induction of active site structural heterogeneity by a two-fold symmetric hemin. Biochemistry. 2006; 45:13875–13888. [PubMed: 17105206]
24. Peng D, Ma L-H, Ogura H, Yang E-C, Zhang X, Yoshida T, La Mar GN. ^{1}H NMR Study of the Influence of Mutation on the Interaction of the C-Terminus with the Active Site in Heme Oxygenase from *Neisseria meningitidis*: Implications for Product Release. Biochemistry. 2010; 49:5832–5840. [PubMed: 20540495]
25. Liu Y, Ortiz de Montellano PR. Reaction Intermediates and Single Turnover Rate Constants for the Oxidation of Heme by Human Heme Oxygenase-1. J. Biol. Chem. 2000; 275:5297–5307. [PubMed: 10681502]
26. Wang J, Ortiz de Montellano PR. The Binding Sites on Human Heme Oxygenase-1 for Cytochrome P450 Reductase and Biliverdin Reductase. J. Biol. Chem. 2003; 278:20069–20076. [PubMed: 12626517]
27. Peng D, Satterlee JD, Ma L-H, Dallas JL, Smith KM, Zhang X, Sato M, La Mar GN. Influence of Substrate Modification and C-Terminal Truncation on the Active Site Structure of Substrate-Bound Heme Oxygenase from *Neisseriae meningitidis*. A ^{1}H NMR Study. Biochemistry. 2011; 50:8823–8833. [PubMed: 21870860]

$watermark-text

$watermark-text

$watermark-text

28. Hernández G, Wilks A, Paolesse R, Smith KM, Ortiz de Montellano PR, La Mar GN. Proton NMR Investigation of Substrate-bound Heme Oxygenase: Evidence for Electronic and Steric Contributions to Stereoselective Heme Cleavage. Biochemistry. 1994; 33:6631–6641. [PubMed: 8204600]
29. Gorst CM, Wilks A, Yeh DC, Ortiz de Montellano PR, La Mar GN. Solution ^{1}H NMR investigation of the molecular and electronic structure of the active site of substrate-bound human heme oxygenase: the nature of the distal hydrogen bond donor to bound ligands. J. Am. Chem. Soc. 1998; 120:8875–8884.
30. Li Y, Syvitski RT, Chu GC, Ikeda-Saito M, La Mar GN. Solution ^{1}H NMR investigation of the active site molecular and electronic structures of the substrate-bound, cyanide-inhibited bacterial heme oxygenase from *C. diphtheriae*. J. Biol. Chem. 2003; 279:6651–6663. [PubMed: 12480929]
31. Smith KM, Fujinari EM, Langry KC, Parish DW, Tabba H. d. Manipulation of Vinyl Groups in Protoporphyrin-IX: Introduction of Deuterium and Carbon-13 Labels for Spectroscopic Studies. J. Am. Chem. Soc. 1983; 105:6638–6646.
32. Smith KM, Craig GW. Porphyrin Synthesis Through Tripyrrins: An Alternate Approach. J. Org. Chem. 1983; 48:4302–4306.
33. Ogura H, Evans JP, Peng D, Satterlee JD, Ortiz de Montellano PR, La Mar GN. The Orbital Ground State of the Azide-Substrate Complex of Human Heme Oxygenase Is an Indicator of Distal H-Bonding: Implications for the Enzyme Mechanism. Biochemistry. 2009; 48:3127–3132. [PubMed: 19243105]
34. Zeng Y, Caignan GA, Bunce RA, Rodriguez JC, Wilks A, Rivera M. Azide-inhibited Bacterial Heme Oxygenases Exhibit an S=3/1 $(d_{xz},d_{yz})^3$ $(d_{xy})^1$ $(d_z{}^2)^1$ Spin State: Mechanistic Implications for Heme Oxidation. J. Am. Chem. Soc. 2005; 127:9794–9807. [PubMed: 15998084]
35. Ma L-H, Liu Y, Zhang X, Yoshida T, La Mar GN. ^{1}H NMR study of the effect of variable ligand on heme oxygenase electronic and molecular structure. J. Inorg. Biochem. 2009; 103:10–19. [PubMed: 18976815]
36. La Mar, GN.; Satterlee, JD.; de Ropp, JS. NMR of Hemoproteins. In: Kadish, KM.; Smith, KM.; Guilard, R., editors. The Porphyrins Handbook. Academic Press; San Diego: 2000. p. 185-298.
37. Smith KM, Pandey RK, Tabba HD. Syntheses of Derivatives of Protoporphyrin-IX Regioselectively Enriched in the Propionic Side Chains with Carbon-13. J. Chem. Res., Synop. 1986:402–403.
38. Hauksson JB, La Mar GN, Pandey RK, Rezzano IN, Smith KM. NMR Study of Heme Pocket Polarity/Hydrophobicity of Myoglobin Using Polypropionate-Substituted Hemins. J. Am. Chem. Soc. 1990; 112:8315–8323.
39. Kikuchi A, Park SY, Miyatake H, Sun D, Sato M, Yoshida T, Shiro Y. Crystal structure of rat biliverdin reductase. Nature Struct. Biol. 2001; 8:221–225. [PubMed: 11224565]
40. Jeener J, Meier BH, Bachmann P, Ernst RR. Investigation of Exchange Processes by Two Dimensional NMR Spectroscopy. J. Chem. Phys. 1979; 71:4546–4553.
41. Griesinger C, Otting G, Wüthrich K, Ernst RR. Clean TOCSY for ^{1}H Spin System Identification in Macromolecules. J. Am. Chem. Soc. 1988; 110:7870–7872.
42. Wishart DS, Bigam CG, Holm A, Hodges RS, Sykes BD. 1H, 13C and 15N Random Coil Chemical Shifts of the Common Amino Acids: I. Investigation of Nearest Neighbnor Effects. J. Biomol. NMR. 1995; 5:67–81. [PubMed: 7881273]
43. Zhu W, Willks A, Stojiljkovic I. Degradation of heme in gram-negative bacteria: the product of the hemO gene of Neisseriae is a heme oxygenase. J. Bacteriol. 2000; 182:6783–6790. [PubMed: 11073924]
44. Wüthrich, K. NMR of Proteins and Nucleic Acids. Wiley & Sons; New York: 1986.
45. Bertini I, Luchinat C. NMR of Paramagnetic Substances. Coord. Chem. Rev. 1996; 150:1–296.
46. Zhu W, Li Y, Wang J, Ortiz de Montellano PR, La Mar GN. Solution NMR study of environmental effects on substrate seating in human heme oxygenase; Influence of polypeptide truncation, substrate modification and axial ligand. J. Inorg. Biochem. 2006; 100:97–107. [PubMed: 16337271]
47. Kolczak U, Hauksson JB, Davis NL, Pande U, de Ropp JS, Langry KC, Smith KM, La Mar GN. 1H NMR investigation of the role of intrinsic heme versus protein-induced rhombic perturbations

on the electronic structure of low-spin ferrihemoproteins: Effect of heme substituents on heme orientation in myoglobin. J. Am. Chem. Soc. 1999; 121:835–843.

48. Shokhirev NV, Walker FA. The Effect of Axial Ligand Plane Orientation on the Contact and Pseudocontact Shifts of Low-spin Ferriheme Proteins. J. Biol. Inorg. Chem. 1998; 3:581–594.
49. Zhu W, Wilks A, Stojiljkovic I. Degradation of Heme in Gram-Negative Bacteria: the Product of the hemO Gene of Neisseriae Is a Heme Oxygenase. J. Bacteriol. 2000; 182:6783–6790. [PubMed: 11073924]

$watermark-text

$watermark-text

$watermark-text

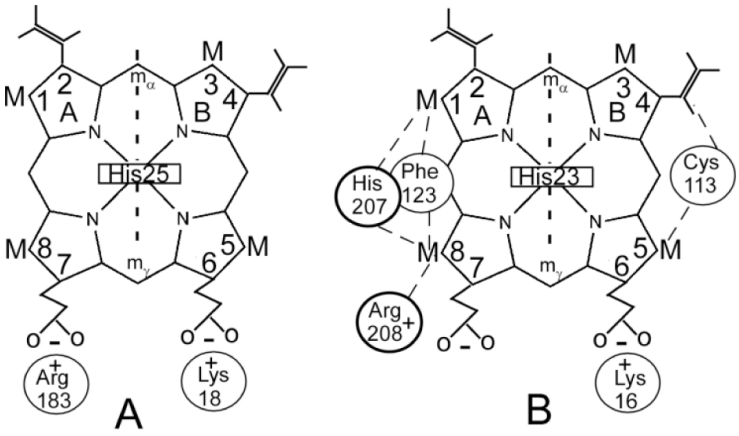

Figure 1.

Orientation of native protohemin-IX within the active site of: (**A**) human HO (8), hHO, showing the key salt bridges of the 6-propionate with the side chain of Lys18 and the 7-propionate with the side chain of Arg183; and (**B**) *Nm*HO (9, 11) showing the conserved salt bridge between the 6-propionate and Lys16, as well as two residues, Cys113, Phe123, key to determining the orientation of substrate in the active site. The contacts of two residues not detected in the crystal structure, His207 with M_1 and M_8 and Arg208 with M_8, are also shown in bold.

$watermark-text
$watermark-text
$watermark-text

$watermark-text

$watermark-text

$watermark-text

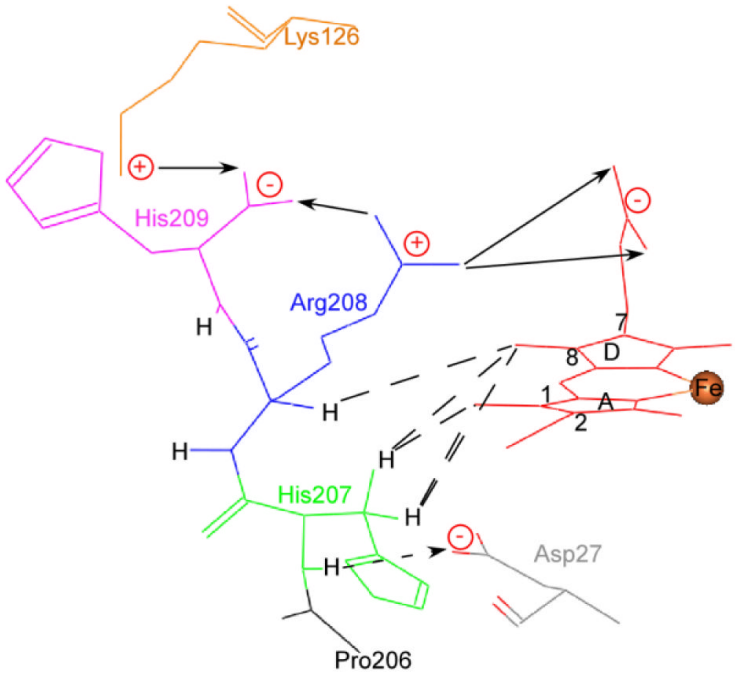

Figure 2.

Proposed molecular model (24) for the C-terminus of substrate-bound *Nm*HO determined by limited energy minimization based on the proposed donor-acceptor interactions (arrows) His207 (green) peptide NH H-bond donor to carboxylate of Asp27 (gray) and the Arg208 (blue) guanidyl group salt bridges to the carboxylates of the 7-propionate (red) and C-terminal His209 carboxylate, which in turn, is an acceptor to the side chains of both Lys126 and Arg208.

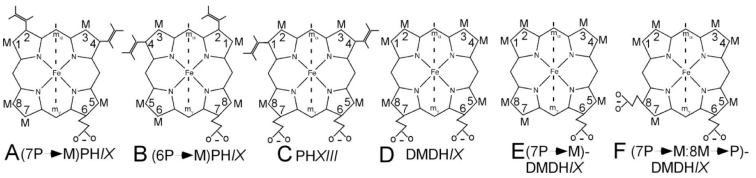

Figure 3.

Structure and labeling of modified hemins relevant to the present study (M = methyl); the orientation of the vinyls groups relative to the adjacent methyl on the same pyrrole is shown as deduced by NOESY cross peaks in solution. (**A**) 7-de-propionate-,7-methyl-protohemin-IX, (7P→M)PH*IX*; (**B**) 6-de-propionate-,6-methyl-protohemin-IX, (6P→M)PH*IX*; (**C**) protohemin-XIII, PH*XIII*; (**D**) 2-,4-dimethyldeuterohemin-IX, DMDH*IX*; (**E**) 7-de-propionate-,7-methyl-2-,4-dimethyldeuterohemin-IX, (7P→M)DMDH*IX*; (**F**) 7-de-propionate-,7-methyl, 8-de-methyl-,8-propionate-2-,4-dimethyldeuterohemin-IX, (7P→M: 8M→P)DMDH*IX*. The orientations of the substrates, relative to the protein matrix, are depicted as found in the active site shown in Figure 1B, and the determined vinyl orientations are shown at *cis* (vinyl H_β next to methyl on the same pyrrole) or *trans* (vinyl H_α next to methyl on the same pyrrole). The arbitrary labeling of the pyrrole positions in two-fold symmetric PH*XIII* and in the DMDH*IX* derivatives is selected so as to correspond to the same number position of PH*IX* in the crystal structure.

$watermark-text
$watermark-text
$watermark-text

$watermark-text

$watermark-text

$watermark-text

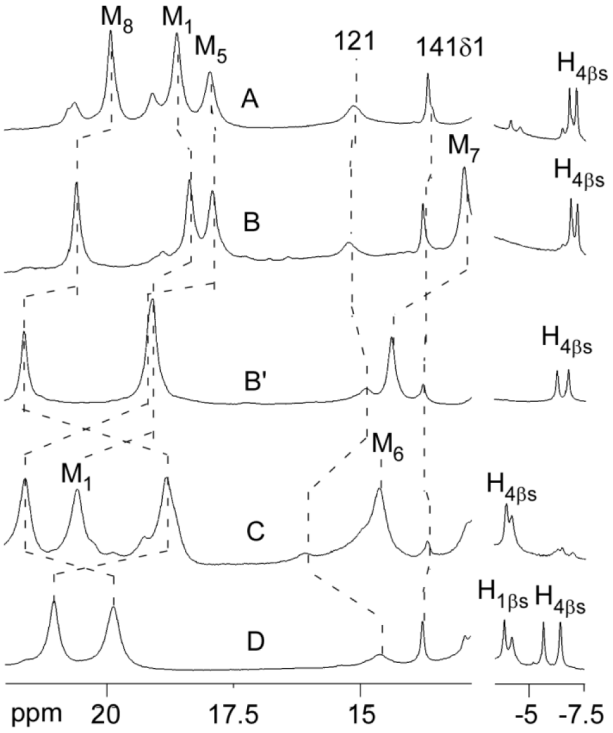

Figure 4.

Resolved portions of the 600 MHz ^{1}H NMR reference spectra, in ^1H_2O, 50 mM phosphate, 75 mM azide, pH 7.1 at 25°C, for: (**A**) WT *Nm*HO-PH*IX*-N_3; (**B**) WT *Nm*HO-(7P→M)PH*IX*-N_3; (**C**) WT *Nm*HO-(6P→M)PH*IX*-N_3; and (**D**) WT *Nm*HO-PH*XIII*-N_3. The spectrum for the "aged" or C-terminal cleaved *Nm*HO complex, *Nm*HO^X-(7P→M)PH*IX*-N_3, is shown in (**B'**).

$watermark-text

$watermark-text

$watermark-text

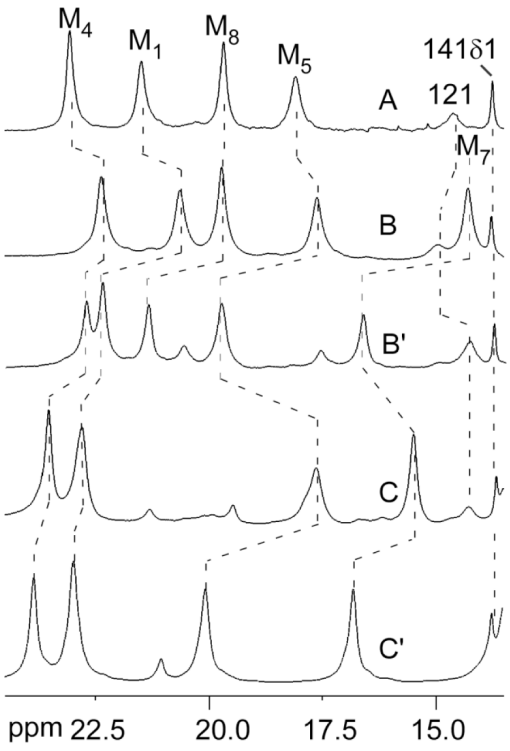

Figure 5.

Resolved portions of the 600 MHz ^{1}H NMR reference spectrum, in ^1H_2O, 50 mM phosphate, 75 mM azide, pH 7.1 at 25°C for: (**A**) WT *Nm*HO-DMDH*IX*-N_3; (**B**) WT *Nm*HO-(7P→M)DMDH*IX*-N_3; and (**C**) WT *Nm*HO-(7P→M:8M→P)DMDH*IX*-N_3. The NMR spectra of the "degraded" or C-terminal cleaved complexes, *Nm*HO^X-(7P→M)DMDH*IX*-N_3, and *Nm*HO^X-(7P→M:8M→P)DMDH*IX*-N_3, are shown in (**B**') and (**C**'), respectively.

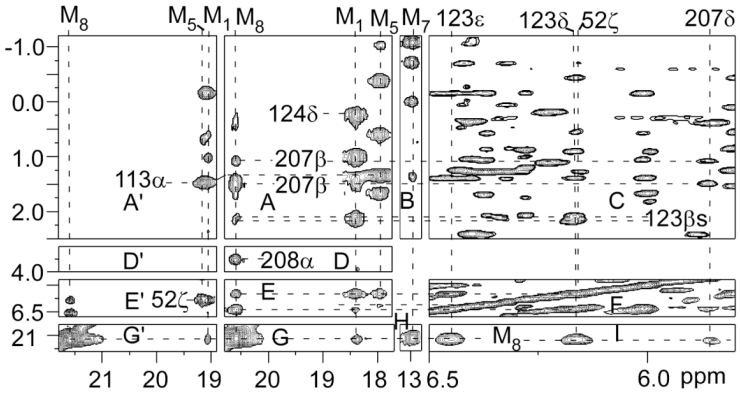

Figure 6.

Resolved portions of the 600 MHz ^{1}H NMR NOESY spectrum, in ^1H_2O, 50 mM phosphate, 75 mM azide, pH 7.1 at 25°C for WT *Nm*HO-(7P→M)PH*IX*-N_3; illustrating key intra-substrate (**A**, **B**, **G**, **H**), substrate residue contacts (**A**, **C**, **D**, **E**, and **I**) for Phe52, Cys113, Phe123, Leu124, His207 and Arg208, and intra-residue contacts (**C**, **F**) for His207 that uniquely assign the substrate and determine the orientation of the substrate in the pocket. Noted are the His207 $C_\beta H$ and $C_\delta H$ contact with M_8 (**E**, **I**) and His207 with M_1 (**E**). Panels (**A**', **D**', **E**' and **G**') for the C-terminal cleaved complex *Nm*HO^X-(7P→M)PH*IX*-N_3 exhibit the same data as panels **A**, **B**, **D**, **E**, **G**, **H** for the WT complex; except for the loss of the His207 and Arg208 cross peaks to M_8/M_1. All panels except **C**, **F** and **I** utilize 45 ppm bandwidth, 2.5 s^{-1} repetition rate and 45° phase-shifted sine-bell apodization; panels **C**, **F** and **I** utilize 20 ppm bandwidth, 1.0 s^{-1} repetition rate and 30° phase-shifted sine-bell apodization.

$watermark-text
$watermark-text
$watermark-text

$watermark-text

$watermark-text

$watermark-text

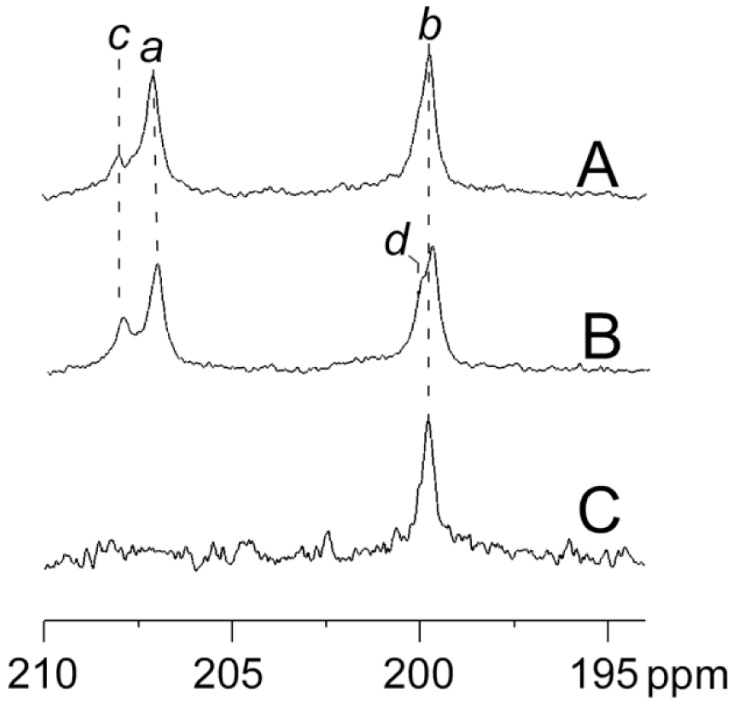

Figure 7.

Portion of the 151 MHz ^{13}C NMR reference spectrum for the carboxylate chemical shift window for: (**A**) ~90% WT *Nm*HO-(6-,7-^{13}CO $^{-}_{2}$)$_2$PH*IX*-H$_2$O, ~10% C-terminal cleaved *Nm*HO^{X}-(6-,7-^{13}CO $^{-}_{2}$)$_2$PH*IX*-H$_2$O; (**B**) ~70% WT *Nm*HO-(6-,7-^{13}CO $^{-}_{2}$)$_2$PH*IX*-H$_2$O, ~30% C-terminal cleaved *Nm*HO^{X}-(6-,7-^{13}CO $^{-}_{2}$)$_2$PH*IX*-H$_2$O; and (**C**) ~75% WT *Nm*HO-(6-^{13}CO $^{-}_{2}$)PH*IX*-H$_2$O, ~25% C-terminal cleaved *Nm*HO^{X}-(6-^{13}CO $^{-}_{2}$)PH*IX*-H$_2$O, which assign peaks *a* and *b* to the 7- and 6-propionate carboxylates, respectively, in the WT *Nm*HO complex, and peaks *c* and *d* to the 6- and 7-carboxylates, respectively, in the C-terminal cleaved *Nm*HO^{X} complex.

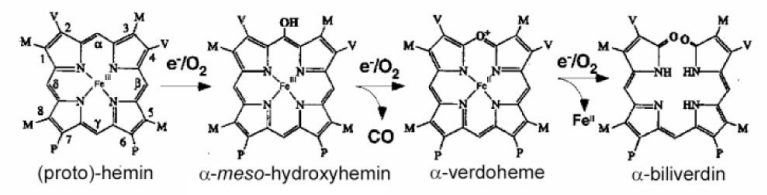

Scheme 1.

$watermark-text
$watermark-text
$watermark-text

$watermark-text $watermark-text $watermark-text

Table 1

Chemical shifts for variable substrates in azide complexes of WT *Nm*HO[a)]

Substrate[b)]	**PH*IX***[c),d)]	**PH*IX***[d),e)]	**(6P→M)-PH*IX***	**(7P→M)-PH*IX***	**DMDH-*IX*** [c)]	**(7P→M)-DMDH-*IX***	**(7P→M:-8M→P)-DMDH*IX***
Peak[e)]							
$M_1(H_{1\alpha})$[f)]	18.68	19.85	20.55	18.34	21.42	20.63	22.90
$M_2(H_{2\alpha})$	(10.32)	(10.22)	(10.75)	(9.04)	10.10	10.62	10.10
M_3	7.60	7.60	8.45	7.66	11.39	?	11.80
$M_4(H_{4\alpha})$	(11.78)	(18.60)	(18.65)	(11.82)	23.00	22.35	23.64
M_5	18.02	20.65	21.57	17.90	18.05	17.60	17.84
M_6	-		14.58	-	-	-	-
M_7	-		-	12.95	-	14.29	15.70
M_8	20.00	19.12	18.79	20.57	19.67	19.70	-
$H_{6\alpha 1}$	9.62	-	-	9.78	8.73	8.38	9.90
$H_{6\alpha 2}$	2.00	-		1.65	5.35	4.06	5.40
$H_{7\alpha 1}$	9.82	10.13	9.38	-	12.17	-	-
$H_{7\alpha 2}$	5.65	2.50	3.25	-	6.70	-	-
$H_{8\alpha 1}$	-	-	-	-	-	-	13.81
$H_{8\alpha 2}$	-	-	-	-	-	-	8.30
His23 $C_{\beta 1}H$	12.56	12.67	12.74	12.65	12.65	12.85	12.77
His23 $C_{\beta 2}H$	9.68	9.78	9.77	9.85	9.28	9.68	9.25

[a)] Chemical shifts in ppm, referenced to DSS, in ^1H_2O, 50 mM phosphate, 75 mM azide, pH ~7.1 and 25°C.

[b)] Substrate structures and proton labels are shown in Figure 3.

[c)] Crystallographic orientation, as in Figure 1B.

[d)] Orientation reversed about the α,γ-meso axis relative to that in the crystal; data taken from Ref. (24).

[e)] Orientation rotated 180° about the α,γ-meso axis relative to that in the crystal.

$watermark-text

$watermark-text

$watermark-text

[f] Vinyl H_α chemical shifts are given in parentheses; vinyl and propionate CβH chemical shifts are provided in Supporting Information, Tables S1 and S2.